scientific reports

Check for updates

OPEN

Ring of capillary actuators as trap, tweezers and ratchet for floating particles

Jean Metzmacher, Megan Delens & Nicolas Vandewalle✉

The manipulation of small floating objects represents a crucial step in mesoscale and microfabrication, or the self-aggregation of particles into functional devices. These tiny objects placed at a liquid-air interface interact due to the local liquid slopes created by their menisci. In this study, we present Dipolar Capillary Actuators (DCA), which can modify the local slope of the interface on demand thanks to the magnetic and capillary torque balance. We experimentally characterize these systems and provide a model to describe their ability to alter liquid slopes. These tiny DCA devices can attract or repel a large range of floating particles with various size, shape and wettability. We present a proof-of-concept system comprising six DCAs arranged in a ring that serves as a capillary trap, tweezers, and ratchet.

With the advancement of knowledge and technologies, an increasing number of elements with diverse compositions, shapes, and scales must be manipulated as building blocks for complex structures. Optical[1,2] and acoustic[3–5] traps and tweezers have proven effective for trapping and manipulating nanoscopic and mesoscopic objects, respectively, and are already used in microfabrication technologies[6–8]. These methods rely on the fundamental principle that particles follow a gradient: the electric field gradient of light in the optical case and the pressure gradient in the acoustic case.

For microscopic to mesoscopic floating particles, a height gradient provides interactions through gravity, leading to capillary interactions[9]. When a particle floats on a surface tilted by another particle or a wall meniscus, the resulting force is no longer perpendicular to the surface, causing a net movement along the surface. Consequently, light particles, such as bubbles, move upward along the meniscus, following the height gradient, while heavier particles denser than the liquid move downward along the interface slope[9,10]. This principle, first proposed by Nicolson[9], implies that the interaction potential mirrors the liquid profile, explaining why floating particles like bubbles, droplets, or even cereals naturally aggregate[10]. Since capillary-driven self-assembly relies on gravity and can be attractive or repulsive, orientational effects can occur[11]. This phenomenon is crucial for the effective self-assembly of various components and has evolved into a sophisticated method for constructing minuscule structures[12–20]. When floating components have magnetic or electric properties and are combined with external fields, these self-assemblies can form floating crystals[21–25], applicable in particle capture and transport, low-Reynolds mixing[26], and even low-Reynolds swimming[27].

Inspired by optical, acoustic, and capillary manipulation methods, Zeng *et al.*[28] proposed 3D-printed capillary machines that function like capillary tweezers to manipulate floating objects inside a vertical channel, with cross-section wettability and shape varying with height. The boundaries and interactions change by altering the liquid height, enabling object movement. They successfully braided micrometer-scale filaments. Recently, we developed 3D-printed arrangements of spines piercing the water to precisely control the liquid landscape, efficiently manipulating floating objects in three dimensions[29]. The next step involves actuating these capillary machines to dynamically change the equilibrium position of particles and control their motion, similar to optical and acoustic traps and tweezers.

In this article, we propose an actuated capillary machine that does not require specific material properties or chemical modification of wettability. We introduce the Dipolar Capillary Actuator (DCA), which can controllably deform a fluid-fluid interface using an induced magnetic field. The magnetic field tilts the device, creating a positive liquid slope on one side and a negative slope on the other, forming a capillary dipole that attracts or repels neighboring particles. We demonstrate how multiple capillary actuators can be arranged in a ring to function as a capillary trap, capillary tweezers, and a capillary ratchet that induces rotary motion in one direction while preventing it in the opposite direction. This one-directional movement is achievable due to an asymmetric energy landscape[30], made possible by the dipolar property of our DCA.

GRASP, Institute of Physics B5a, University of Liège, B4000 Liège, Belgium. ✉email: nvandewalle@uliege.be

Results

Dipolar capillary actuator

The shape of a particle's meniscus is dictated by its wettability, buoyancy, shape, and surface state. The triple-phase contact line may or may not be pinned depending on the surface roughness or chemical heterogeneity of the particle. The liquid interface can be significantly modified by varying one of these parameters. In earlier works, we used the curvature of objects to control the shape of the contact line, thereby influencing the final capillary self-assembly[31]. We also dynamically adjusted this curvature using shape-memory polymers[14] or by embedding small magnets in flexible objects to deform them under a magnetic field[13]. This actuation of floating particles, termed smart objects, enabled dynamic changes in self-assembling patterns.

This study aims to manipulate floating particles, whether smart or not, independently of their intrinsic properties by controlling the liquid slope around them. Building on our previous studies, we designed an actuator capable of progressively and continuously deforming the interface, creating a concave meniscus on one side and a convex meniscus on the other. When the contact line exhibits multiple lobes, these deformations are referred to as capillary multipoles, similar to how electrostatic fields can exhibit monopoles, dipoles, and higher-order components[32–35]. Due to the two lobes of opposite curvature it generates, we call our device the Dipolar Capillary Actuator (DCA). The DCA comprises three components: a floater, a support, and a coil (see Fig. 1 (a)). The floater consists of a 4.5 mm diameter disk with two edge notches and a central protrusion holding a 1 mm thick magnet aligned parallel to the disk. The support maintains the floater in a fixed position and consists of two pillars that pass through the floater's notches. The coil surrounds the floater's protrusion and the pillars. When the DCA is placed in a liquid, the floater naturally assumes a horizontal position at the surface, as shown in Fig. 1 (b). The contact line is pinned around the DCA perimeter. When current flows through the coil, a vertical magnetic field is generated around the floater's magnet, which, therefore, experiences a magnetic torque that attempts to align the magnetic moment with the field. However, surface tension forces and gravity oppose this torque. The balance between these opposing forces establishes a tilt angle $_{\alpha}$, causing the interface to deform, forming two lobes of opposite curvature. (see Fig. 1 (c)). Reversing the field changes the floater's orientation, inverting the curvature (Fig. 1 (d)).

The liquid profile around the object should satisfy the Young-Laplace equation. When the interface slope is small ($\ll 45^{\circ}$), the Young-Laplace equation can be linearized, and its solution can be expressed as a Fourier multipole expansion, which is equivalent to summing monopole, dipole, quadrupole, and higher-order components. The interface deformation h around an object with an anisotropic contact line is given by[32–34,36]:

$$h(r,\theta) = \sum_{m=0}^{\infty} Q_m K_m(r/\lambda)\cos\left[m(\theta-\theta_m)\right] \tag{1}$$

where (r,θ) are the cylindrical coordinates centered on the particle, Q_m is a constant of integration called capillary charge of the mth order, characterizing the depth of the deformation, K_m is the modified Bessel

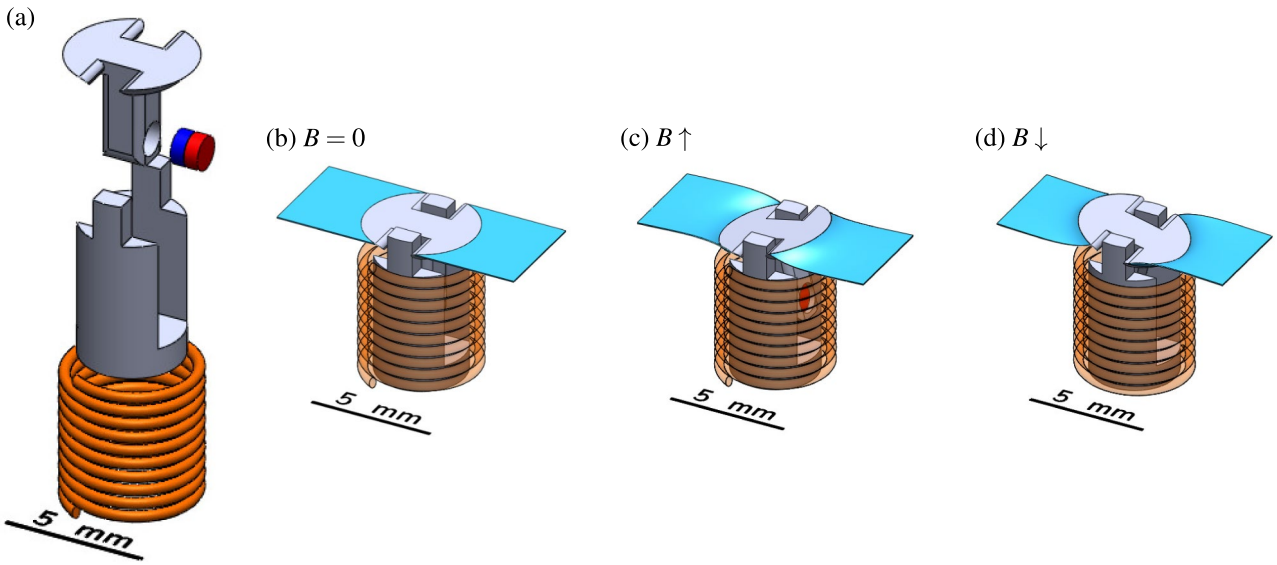

Fig. 1. Illustration of the Dipolar Capillary Actuator (DCA). A floater containing a small magnet is placed at the liquid interface above a support that keeps this floater in a fixed position. A coil surrounds these components. A vertical magnetic field can be created around the magnet by injecting a current into the coil. The magnet tries to align itself with the magnetic field, which tilts the floater and deforms the interface. (**a**) Exploded view of the DCA. (**b**) Natural position of the floater on an undisturbed liquid interface. As its center of mass is just below the center of the disk, it remains horizontal. (**c**) Deformation of the interface when an upward magnetic field is applied on the floater. (**d**) The deformation is inverted when the field is reversed.

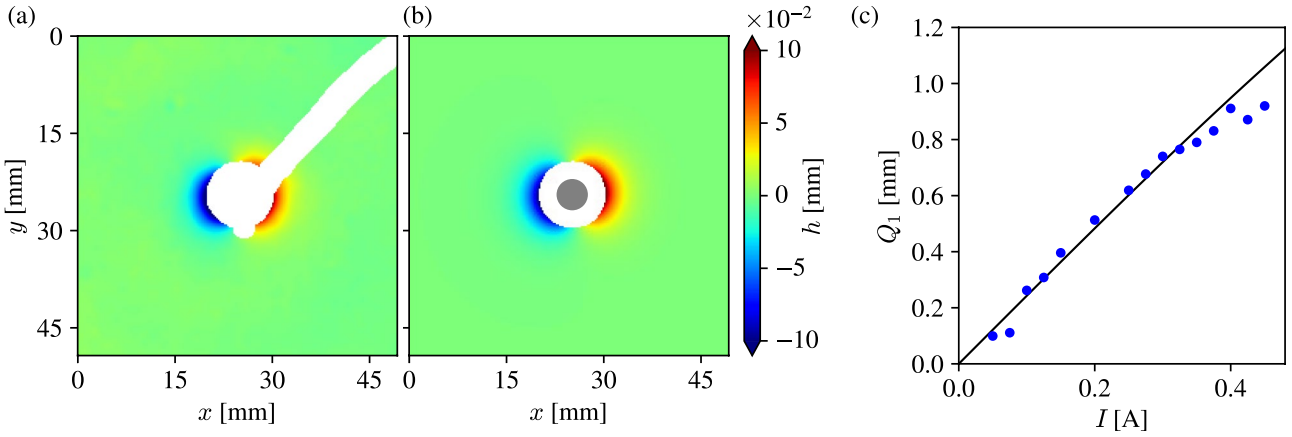

Fig. 2. Deformation of the interface around a DCA caused by the tilting of the floater when a current is injected into the coil. The resulting capillary multipole presents two lobes of opposite signs corresponding to a dipole. (**a**) Surface profile around a DCA measured by the Fast Checkerboard Demodulation method. A current of 0.275 A powers the DCA. The white line starting from the upper right corner corresponds to the cable that powers the DCA. (**b**) Surface profile around a DCA as fitted with Eq. 1 with $m = 1$. (**c**) Measured capillary charge Q_1 of the DCA as a function of the current I injected into the coil. The curve represents the evolution of the charge Q_1 as a function of I as predicted by the numerical minimization of Eq. 2.

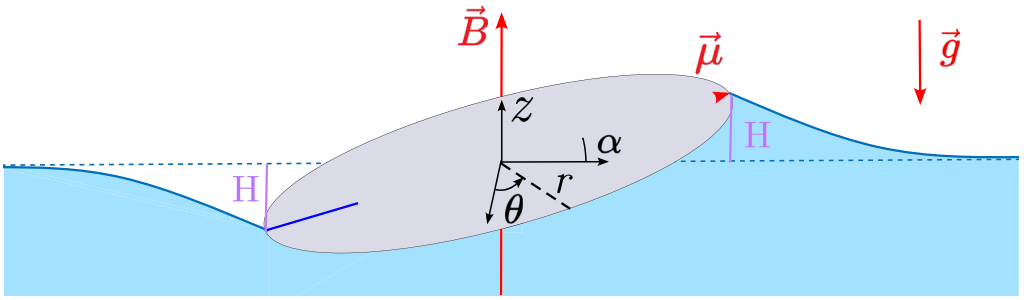

Fig. 3. Sketch of a floating tilted disk (grey) with an angle α. The disk is parallel to a magnetic moment $\vec{\mu}$. The tilt induces a positive meniscus on one side, while a negative meniscus is seen on the other, providing a capillary dipole.

function of the second kind and mth order, λ is the capillary length, the characteristic length scale at which gravitational forces and surface tension forces are balanced, and θ_m is the orientation of the mth order. The capillary length is defined as $\lambda = \sqrt{\gamma/\rho g} \approx 2.7$ mm for water-air interfaces where γ is the surface tension, ρ is the liquid density and g is the gravitational acceleration.

The deformed interface around the DCA exhibits two lobes of opposite signs, corresponding to a dipole ($m = 1$ in Eq. 1). Because the DCA floater is thin, has a density close to the water, and presents a pinned contact line, the monopolar term $m = 0$ can be neglected. An external torque must be applied to the particle to produce a distortion with a dipole component[36–38]. Previous investigations have reported dipolar interfaces by applying a magnetic field on magnetic particles[24,39–42] or when particles are driven along fluid interfaces[43]. In our case, the external torque is generated by the magnetic field created by the coil acting on the embedded magnet. We measured this deformation using the Fast Checkerboard Demodulation (FCD) method[44,45] and fitted the dipolar expression of Eq. 1. As shown in Figs. 2 (a) and (b), our data are in good agreement with the theoretical profile. The dipolar capillary charge created by the DCA is controlled by the magnetic field produced by the coil, which is proportional to the current injected into it. To determine how the surface deformation can be tuned with the DCA, we measured the dipolar charge $\pm Q_1$ as a function of the current. The charge was obtained by imaging the interface with the FCD method and fitting Eq. 1 to the data, as in Fig. 2 (b). The evolution of the measured capillary charge Q_1 as a function of the current I injected into the DCA is shown in Fig. 2 (c). As expected, the capillary dipolar component increases with I since the contact line is pinned on the DCA's floater perimeter, which tilts more as I increases. Saturation is, however, observed because the surface and gravitational energies resisting the magnetic energy evolve more rapidly than the latter with the tilt angle α as shown in Fig.3.

The evolution of the interface with the current can be predicted by minimizing the free energy of the DCA. The free energy difference of the DCA between its flat equilibrium configuration and its tilted orientation can be written as

$$\Delta E = \gamma \Delta A + \rho \Delta V g \frac{H}{2} - \mu B \sin\alpha \tag{2}$$

where, in order, the differences in surface energy, gravitational energy, and magnetic energy are considered. The increased air-water interface area ΔA is given by[38,39]

$$\Delta A = \frac{1}{2}\int_0^{2\pi}\int_{R\cos\alpha}^{\infty} (\nabla h)^2 r \; dr d\theta = \frac{Q_1^2}{2}\int_0^{2\pi}\int_{R\cos\alpha}^{\infty} r\left(\frac{\left(-K_0\left(\frac{r}{\lambda}\right) - K_2\left(\frac{r}{\lambda}\right)\right)^2\cos^2\theta}{4\lambda^2} + \frac{K_1\left(\frac{r}{\lambda}\right)^2\sin^2(\theta)}{r^2}\right) dr d\theta, \tag{3}$$

where we also assume a small slope. The volume ΔV displaced by the meniscus is described by

$$\Delta V = 2\int_{-\pi/2}^{\pi/2}\int_{R\cos\alpha}^{\infty} r Q_1 K_1\left(\frac{r}{\lambda}\right)\cos\theta \; dr d\theta, \tag{4}$$

and H is the maximal height/depth of the meniscus that relates the tilt angle α and the dipolar capillary charge Q_1 and is given by

$$H = Q_1 K_1\left(\frac{R\cos\alpha}{\lambda}\right) = R\sin\alpha \Leftrightarrow Q_1 = \frac{R\sin\alpha}{K_1\left(\frac{R\cos\alpha}{\lambda}\right)} \tag{5}$$

The product μB in the magnetic energy is the product of the magnetic moment μ of the embedded permanent magnet and the magnetic field B produced by the current in the solenoid. This product can be rewritten $B_r \Omega n I$ with Br, the magnetic remanent field of the neodymium-based magnet, Ω, its volume, and n, the loop density of the coil found using the Biot-Savart law.

For a given current I, the capillary charge Q_1 and the associated tilt angle α should be as it minimizes the free energy. Integrals in Eqs. 3 and 4 do not have analytical solutions over α. The total free energy must, therefore, be computed and minimized numerically. Injecting Eqs. 3, 4, and 5 in Eq. 2 and numerically minimizing it over α, we predict the tilt angle and the associated capillary charge Q_1 evolution with current I, closely matching our experimental results, as shown in Fig. 2(c).

These results imply that the current can be adjusted to achieve a specific liquid deformation around the DCA. This precise liquid slope control offers a versatile tool for experiments requiring customized liquid boundaries and could extend to broader applications where tailored liquid interfaces are essential.

Capillary trap

While a single DCA can successfully modulate the liquid surface, the extent of this deformation is limited. However, combining multiple DCAs allows the overall liquid landscape to be extended and complexified to become a functional and programmable manipulation tool. As a first example, several DCAs can be arranged in a circular array to create a trap for floating particles. Inside this array, the DCAs' dipoles converge and combine to create a global deformation of the liquid surface. By controlling the dipoles of the DCAs, the interface can be shaped to create an extremum where floating particles can be trapped.

Following Nicolson's method[9], the energy of a particle on a fluid interface is dominated by gravitational potential energy and can be expressed as:

$$E = -2\pi\gamma Q_p h(x,y), \tag{6}$$

where Q_p is the capillary charge of the particle (see Supplementary File S0 for detailed derivation of this equation). A heavy (light) particle with a negative (positive) capillary charge moves down (up) the interface to lower its energy. By creating a valley (hill) at the interface's center, we can trap heavy (light) particles. In our scenario, capillary forces dominate over higher-order interfacial energies, allowing gravitational energy to drive the particle's motion along the curved interface[10,46,47]. Given that the typical distortion length, the capillary length λ, is $2.7\,\mathrm{mm}$ for pure water, the radius of the circular array should be on this order to achieve significant deformation at its center. The inner radius of the trapping device is set to $4.75\,\mathrm{mm}$, slightly above the capillary length, allowing the displacement of millimeter-sized particles over larger distances.

In this array, six DCAs are symmetrically placed. Six is the maximum number of DCAs that can fit around a $4.75\,\mathrm{mm}$ circle. Fewer DCAs could be used to build the trap, but using more DCAs allows for more elaborate interface shapes as more local deformations combine to create the total deformation.

We captured various floating particles at its center to demonstrate the trapping ability of the array of DCAs. The device was placed in water with all DCAs oriented radially and set to the same current, resulting in the same liquid slope. This configuration deforms the interface by creating a valley or a hill, depending on the sign of the dipolar charge of the floaters. These profiles are computed from the theoretical expression of a dipolar capillary charge (Eq. 1 with $m = 1$) and the superposition principle. Fig. 4 (a) shows a simulated interface presenting a valley shape. The black triangle indicates the bottom of this valley, which corresponds to the trap position.

We performed trapping experiments with two types of particles: a solid spherical bead and a droplet of mineral oil. The bead is a 1-millimeter-diameter glass sphere and floats thanks to partial wetting. Being denser than water, its capillary charge Q_p is negative. In the trapping configuration described above, the bead is consequently localized at the center of the trap, as shown in Fig. 4 (b).

We also investigated a small mineral oil droplet placed at the water-air interface. Although many oil droplets tend to spread on water surfaces, mineral oil forms a so-called floating "liquid lens" at equilibrium. This

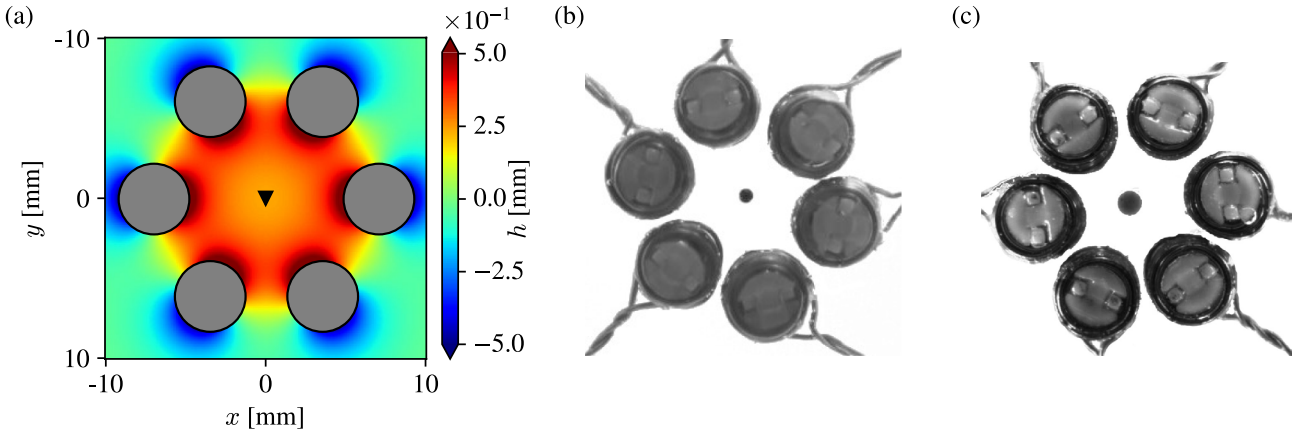

Fig. 4. Trap at the center of a ring of six DCAs oriented radially. The DCAs have all the same capillary charge. (**a**) Simulation of the surface topography with $Q_1 = 0.6\,\mathrm{mm}$. When all the positive poles of the DCAs are towards the center, a minimum (black upside-down triangle) is created inside the tweezers. (**b,c**) Trapping experiments of particles of negative capillary charge floating at the surface of water when a minimum is created at the center of the capillary tweezers. A glass bead of a 1-millimeter radius is trapped at the center (**b**). A mineral oil drop forming a floating "liquid lens" and presenting a small negative curvature, i.e. a small negative Q_p, is trapped at the center as easily as the glass bead (**c**). A blue dye is added to the oil to distinguish the drop from water.

behavior arises from the balance of interfacial tensions at the triple phase contact line: $\gamma \approx 72\,\mathrm{mN/m}$ for the water-air interface, $\gamma_{wo} \approx 50\,\mathrm{mN/m}$ for the water-oil interface and $\gamma_{oa} \approx 30\,\mathrm{mN/m}$ for the oil-air interface. The equilibrium condition $\gamma < \gamma_{wo} + \gamma_{oa}$ is satisfied in our system. Although surfactants are often added to promote the formation of such liquid lenses with oil-water based mixtures, we deliberately avoid them here, as they reduce the capillary length and affect the floatability of the DCA heads.

Manipulating a floating mineral oil droplet is delicate, as any contact with a solid object may rupture the droplet or result in adhesion. Our system is particularly well suited to trap such liquid lenses without direct contact. At equilibrium, liquid lenses present a small negative curvature, i.e. a small negative Q_p, as demonstrated recently theoretically and experimentally by Ravazzoli *et al.*[48]. As a result, they are attracted by a trap with negative curvature, as illustrated in Fig. 4 (c).

Capillary tweezers

In the previous subsection, a capillary trap was achieved at the center of the DCA ring by injecting the same current into each DCA. A step forward is to use the same array of actuators but modify the current of one or several DCAs to move the trap. This allows to manipulate the particle to any position inside the array, transforming the trap into capillary tweezers. Each DCA's dipole intensity can be independently controlled because the entire device is powered by six bi-directional current sources individually driven by a microcontroller.

Figs. 5 (a) - (c) show simulated profiles of the liquid inside the array and the displacement of the trap when the capillary charges of some DCAs are increased. Simulations indicate that the minimum position moves when the charge Q_1 of one or two DCAs is increased.

We conducted experiments to move various floating particles, such as beads and drops, using the previously described array of DCAs. Figs. 5 (d) - (f) show experimental images of the displacement of a mineral oil drop inside the capillary tweezers. As in the previous section, the oil drop forms a floating "liquid lens" which presents a small negative Q_p. The charges on some DCAs were modified as in the simulations in Figs. 5 (a) - (c), and a similar trajectory was observed. The real time movie can be seen in Supplementary Video S1.

These results demonstrate that our capillary tweezers can manipulate floating entities without direct contact. The proposed technique only requires that the floating particle has a capillary charge, i.e. a meniscus. There is no need for special properties such as magnetic or electric ones. This method offers a versatile and programmable way to manipulate a wide range of particles, including solid particles, drops, or bubbles.

Capillary ratchet

The proposed capillary tweezers can also be transformed into a ratchet capable of directional transport of floating particles along the ring formed by the DCAs. A ratchet is commonly defined as a mechanical device that permits continuous linear or rotary motion in one direction while preventing motion in the opposite direction.

To create rotation along the ring, adjacent DCAs should be set in phase opposition and actuated using sinusoidal currents. This configuration creates local minima and maxima in alternation at the edge of the DCAs. After half a period of the current, each previous trap became repellent and vice versa. In the case where all DCAs are oriented radially as in the previous trap and tweezers configurations, the manipulated particle will equiprobably move either to the left DCA or to the right without resulting in a net motion after multiple periods.

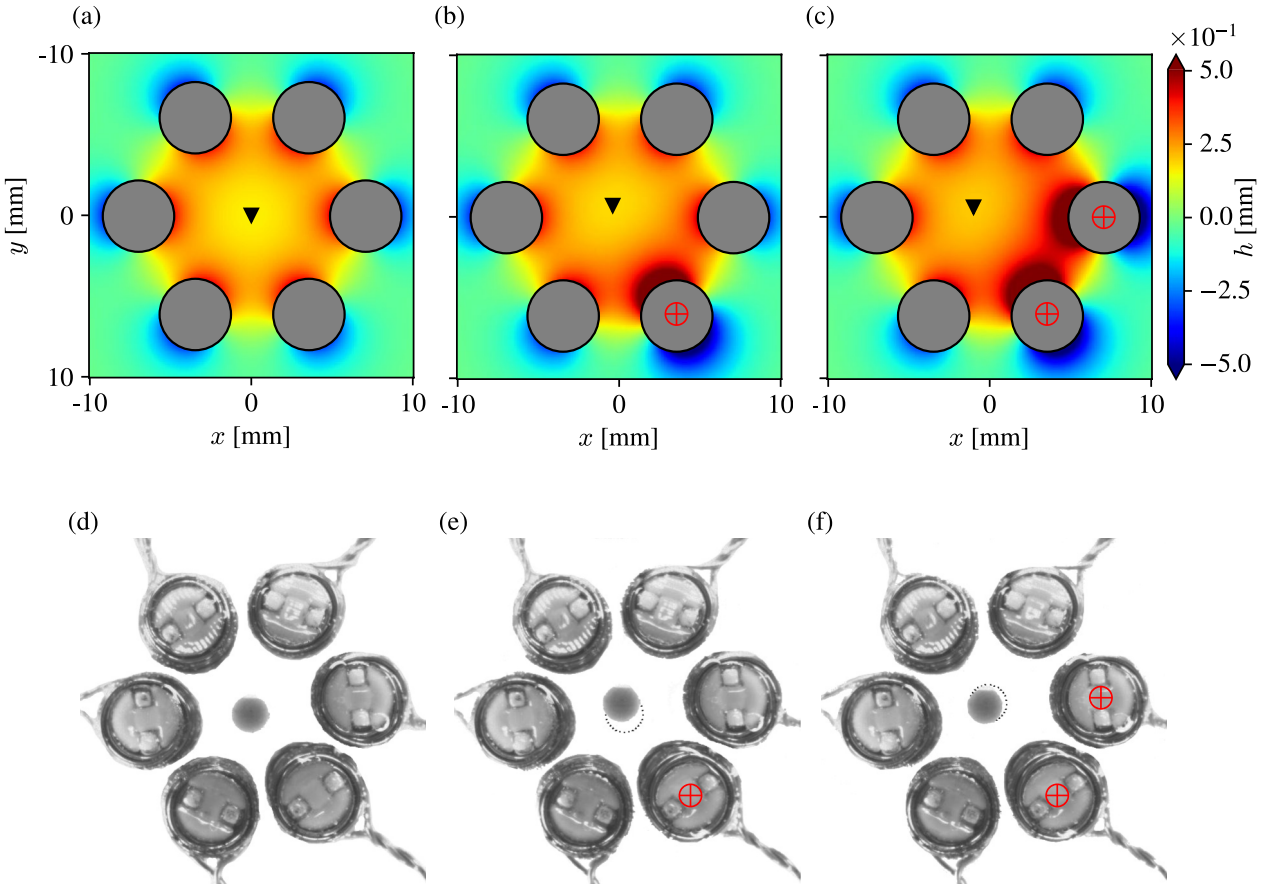

Fig. 5. Displacement of a particle by increasing the charge of some DCAs to modify the position of the trap. (**a-c**) Simulations. The black upside-down triangle indicates the center of the trap. In (**a**), all DCAs have the same charge of $0.4\,\mathrm{mm}$. Then, the capillary charge of some DCAs is increased to $0.8\,\mathrm{mm}$(**b,c**). (**d-f**) Experiment of trapping and moving a mineral oil drop at the surface of water. The oil drop forms a floating "liquid lens" and presents a small negative curvature, i.e. a small negative Q_p. It is therefore attracted by the minimum inside the capillary tweezers. A blue dye is added to the oil to distinguish it from water. In (**d**) all DCAs have similar capillary dipolar charges, the particle is trapped at the center of the capillary tweezers. Then, the charge of some DCAs is increased to displace the drop (**e,f**). The dashed circles represent the position of the particle from the previous step. The DCAs with increased capillary charges are marked by a red "$\oplus$" symbol. The real time movie can be seen in Supplementary Video S1.

The energy landscape along the path should be asymmetrical to create a functional ratchet and ensure that the particle always goes in the same direction. Tilting the orientation of the DCAs from the radial direction creates the required asymmetry in the energy landscape. Here, we turn them 45° counter-clockwise, which is the intermediate orientation between the extreme radial and tangential positions. In this new configuration, the particle will always be attracted to the left DCA after half a period of the current, leading to a general clockwise movement.

A simulation of the interface created by the array of DCAs in this configuration is shown in Figs. 6 (a) and (b) for the extremal current values, respectively. As stated before, the potential energy can be reduced to the height of the interface. Thus, Figs. 6 (a) and (b) show that the potential energy surfaces created by the array of DCAs in this configuration are asymmetrical, meaning that this device can well be considered as a ratchet.

With this proposed ratchet, we performed directional transport experiments of a floating glass bead of $1\,\mathrm{mm}$ radius. We observed that the bead always moves clockwise along the ratchet, as illustrated in Figs. 6 (c) and (d) (see Supplementary Video S2 for the real-time movie). These figures show the opposite gradient of a simulated interface's height and the trajectory of the particle obtained in the experiments. The hashed circles represent the DCAs. The experimental positions of the bead are the filled circles. Its current position is in black, and past positions are in gray. We can observe that the orientation of the DCAs and the resulting positions of local extrema lead to an interface that is no longer symmetrical with respect to the radial direction. By moving to the neighboring DCA on its left, the particle follows the steepest local slope of the interface.

Adjusting the orientation of the DCAs and setting adjacent DCAs in phase opposition allows directional transport of not only a single particle but several particles simultaneously. Moreover, these particles can be of different natures (light or heavy). Indeed, several local minima and maxima are created, and floating objects

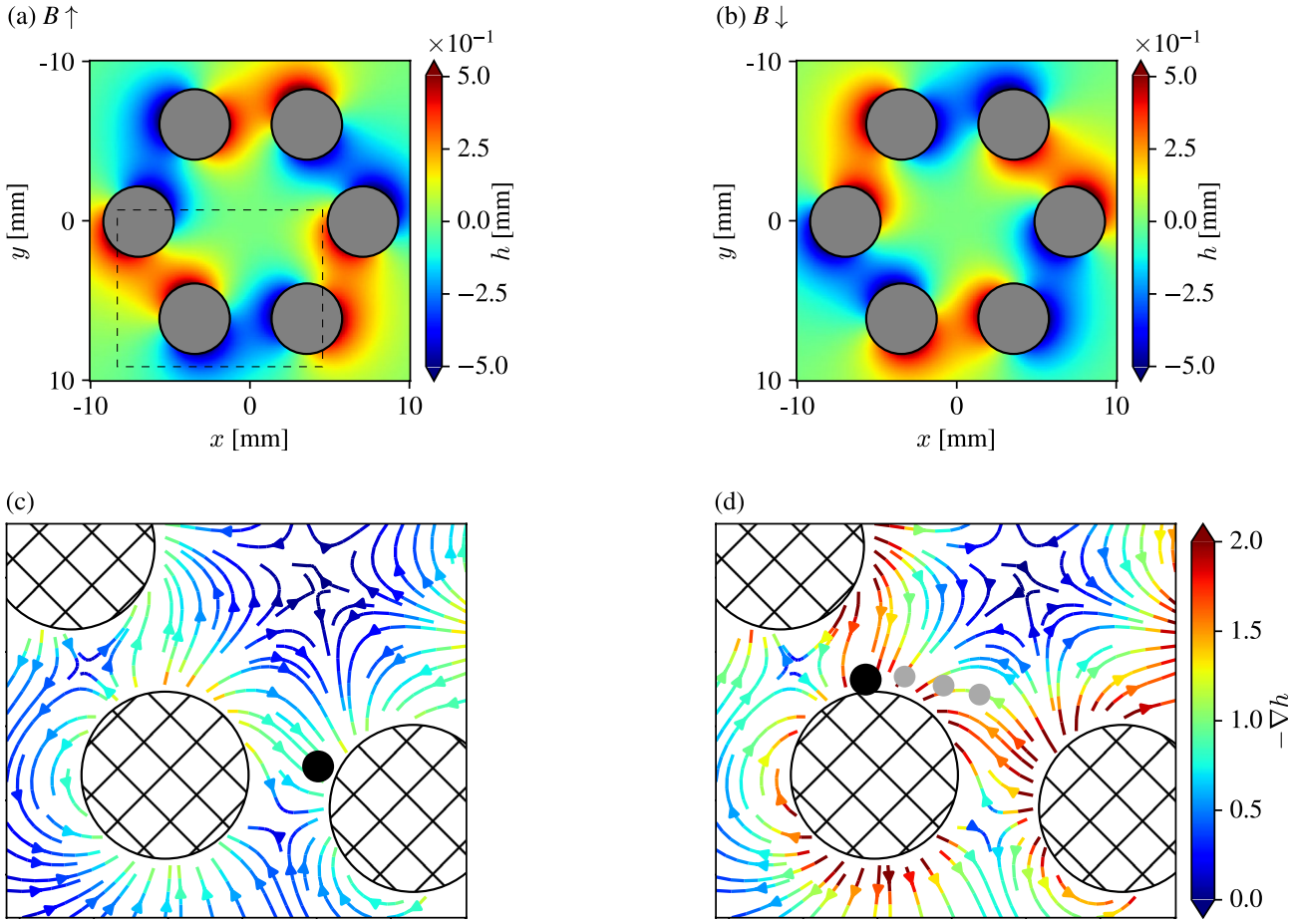

Fig. 6. Directional transport of a $1\,\mathrm{mm}$ floating glass bead inside the ratchet. (**a,b**) Simulations. In the ratchet, adjacent DCAs are in phase opposition and tilted by an angle of 45° from the radial direction. Local minima and maxima are created in alternation along the ring formed by the DCAs. The module of the charges is $0.6\,\mathrm{mm}$. (**c,d**) Experiments. The bead is the black circle, while the gray circles correspond to past positions. Streamlines represent the opposite gradient of the height of the simulated interface computed from the superposition of six dipolar capillary charges, as in (**a,b**). In (**c**), The bead is captured at the local minimum of a DCA. In (**d**), the magnetic field has reversed, and the glass bead fell down the interface in the minimum at the edge of the left DCA. The real-time movie can be seen in Supplementary Video S2.

of both types can be transported. The potential asymmetry guarantees that all particles are displaced in the same direction, regardless of their nature. Fig. 7 shows the simultaneous directional transport of a single bead and a dimer composed of two beads (see Supplementary Video S3 for the real-time movie). The beads of the dimer stick together only by a capillary bridge. In a ring of six DCAs, any particle requires three time periods to complete a full rotation and return to its starting position. The speed of this motion can be adjusted by changing the frequency. However, efficient motion is only possible below a frequency threshold that we can approximate using simple assumptions. Specifically, the displaced object must have enough time to enter the potential field of the adjacent DCA in approximately $T/4$, meaning that this frequency threshold highly depends on the shape, weight and nature of the displaced object. For the DCAs in a ratchet configuration with a current of $0.2\,\mathrm{A}$, a glass bead takes approximately $0.6\,\mathrm{s}$ to move from one DCA to the next. This means that it takes half of this time for the bead to exit the repulsive potential of one DCA and enter the attractive field of the next. Thus, for this setup, the minimum period and maximum frequency for effective movement are approximately $T_{\min} \approx 1.2\,\mathrm{s}$ and $f_{\max} \approx 0.8\,\mathrm{Hz}$, providing an estimate of the magnitude order of the maximal frequency possible to observe ratcheting.

Conclusion

In this paper, we presented Dipolar Capillary Actuators (DCAs) as a programmable and effective tool for manipulating floating particles at fluid-air interfaces. By leveraging the balance of magnetic and capillary forces, these actuators can generate precise liquid deformations, creating capillary dipoles that enable the attraction or repulsion of a large range of particles with various size, shape and wettability.

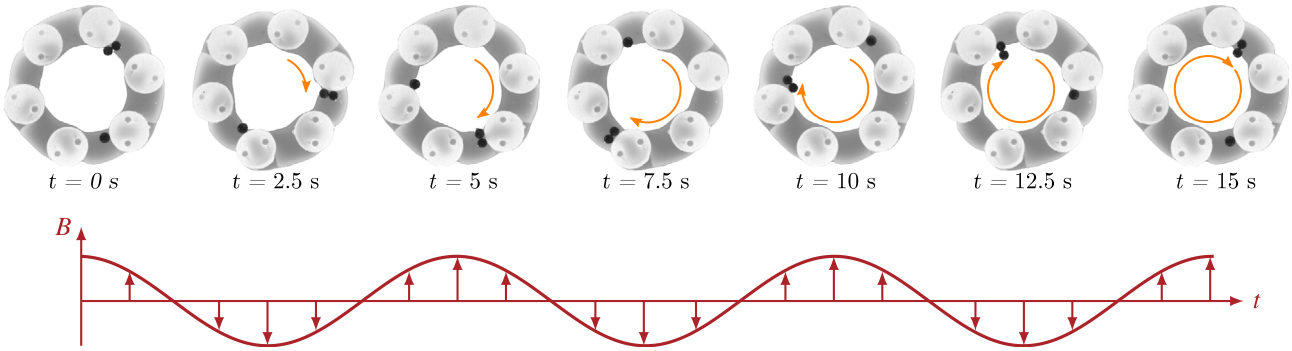

Fig. 7. Simultaneous transport of a single glass bead of 1 mm and a dimer inside the ratchet. The dimer is composed of two glass beads of 1 mm that stick together only by a capillary bridge. A sinusoidal current is injected into the coils of the DCAs. They are tilted from the radial direction by an angle of 45°, and adjacent ones are 180° out of phase and therefore have opposite charges. The frequency of the electric current fixes the transport speed. This experiment sets the frequency to 0.2 Hz. The time between each step motion is, therefore, half the period, $T/2 = 2.5$ s. The real-time movie can be seen in Supplementary Video S3.

Being based on capillary effects, the main limitation of the proposed device should be the size of the particle. For "large" objects, typically in the centimeter range, capillary forces become negligible compared to gravitational and inertial effects, whereas for very small particles, typically in the micrometer range, thermal agitation (Brownian motion) can dominate, counteracting the capillary-driven motion. Other properties, such as particle shape or wettability, could influence the meniscus profile and, consequently, modulate the strength and directionality of the interaction between the actuators and the particle. However, these variations are not expected to suppress the interaction entirely, and should therefore not prevent effective manipulation of the particle.

Using interface simulations and experiments, we demonstrated the ability of a ring of DCAs to function as a capillary trap, tweezers, and ratchet. The ability of the system to dynamically control the liquid surface allowed for real-time trapping, positioning, and transportation of various particles, including solid beads and liquid droplets. In particular, live and reversible modification of the interface and the consequent manipulation represent a step forward compared to existing similar methods[28,29]. Furthermore, the ratchet mechanism introduced provides a directional bias, enabling controlled, unidirectional transport of particles around the actuator array.

Our results show that DCAs offer a highly tunable, contactless approach to particle manipulation, with applications ranging from particle capture and sorting to self-assembly in mesoscale and microfabrication contexts. By eliminating the need for specific material properties, such as magnetic or dielectric characteristics, this method provides a flexible platform for manipulating a broad range of particles. These findings open up new possibilities for designing complex systems in areas such as soft robotics, microelectronics, and microfluidics.

Methods

Fabrication of the DCA

The floater and support of the DCA were designed in SolidWorks and exported in STL files (STL files are given in Supplementary Dataset S4). DCAs were 3D-printed using a PolyJet 3D printer (Stratasys Objet 30). The resin used is similar to ABS plastic (Vero Blue) and has a polymerized density of $\rho_p = 1180$ kg/m^3. This 3D-printing method boasts high precision with an announced resolution of 16 μm in high-quality mode. The support material can be dissolved in water, eliminating any contact point that can alter the surface and increase roughness. Consequently, a smooth contact line is achieved, avoiding additional capillary multipolar effects. We used 1 mm diameter x 1mm long cylindrical Neodymium magnets of grade N45 from Supermagnete. The announced remanent magnetic field for this grade is $1.32 - 1.37$ T. The handmade coils consist of two concentric rows of 11 turns of a 0.4 mm diameter copper wire on a total 7 mm length. The loop radius is 2.5 mm. The rows are glued together. Using Biot-Savart Law, the resulting loop density is 2.398 mm^{-1}.

Experimental details

Water is used in all experiments. The DCAs were placed in the bottom of a Petri dish. A homemade six bi-directional generator was used to power the coils. A microcontroller drives it and uses pulse-width modulation to generate the desired signals. Glass beads were 1 mm in diameter and were placed in the center of the DCAs ring using clean tweezers. Drops of mineral oil were placed on the liquid surface using a syringe. Mineral oil was dyed using silicon coloring. A CCD camera records images and videos from above the experimental setup.

Data availibility

The authors declare that the main data supporting the findings of this study are available within the paper and the supplementary movies S1-S3. Any additional information is available from the corresponding author upon reasonable request.

Received: 3 November 2024; Accepted: 9 June 2025
Published online: 01 July 2025

References

1. Ashkin, A. Acceleration and trapping of particles by radiation pressure. *Physical review letters*. **24**, 156 (1970).
2. Ashkin, A., Dziedzic, J. M., Bjorkholm, J. E. & Chu, S. Observation of a single-beam gradient force optical trap for dielectric particles. *Optics letters*. **11**, 288–290 (1986).
3. Gor'kov, L. On the forces acting on a small particle in an acoustical field in an ideal fluid. *In Soviet Physics Doklady*. **6**, 773 (1962).
4. Wu, J. Acoustical tweezers. *The Journal of the Acoustical Society of America*. **89**, 2140–2143 (1991).
5. Brandt, E. Suspended by sound. *Nature*. **413**, 474–475 (2001).
6. Agarwal, R. et al. Manipulation and assembly of nanowires with holographic optical traps. *Optics express*. **13**, 8906–8912 (2005).
7. Pauzauskie, P. J. et al. Optical trapping and integration of semiconductor nanowire assemblies in water. *Nature materials*. **5**, 97–101 (2006).
8. Marzo, A. & Drinkwater, B. W. Holographic acoustic tweezers. *Proceedings of the National Academy of Sciences*. **116**, 84–89 (2019).
9. Nicolson, M. M. The interaction between floating particles. *Math. Proc. Cambridge Philos. Soc.* **45**, 288–295. https://doi.org/10.1017/S0305004100024841 (1949).
10. Vella, D. & Mahadevan, L. The "Cheerios effect". *Am. J. Phys.* **73**, 817–825. https://doi.org/10.1119/1.1898523 (2005).
11. Danov, K. D. & Kralchevsky, P. A. Capillary forces between particles at a liquid interface: General theoretical approach and interactions between capillary multipoles. *Advances in colloid and interface science*. **154**, 91–103 (2010).
12. Rothemund, P. W. Using lateral capillary forces to compute by self-assembly. *Proceedings of the National Academy of Sciences*. **97**, 984–989 (2000).
13. Metzmacher, J., Poty, M., Lumay, G. & Vandewalle, N. Self-assembly of smart mesoscopic objects. *The European Physical Journal E*. **40**, 1–6 (2017).
14. Vandewalle, N. et al. Switchable self-assembled capillary structures. *Soft Matter*. **16**, 10320–10325 (2020).
15. Lehle, H., Noruzifar, E. & Oettel, M. Ellipsoidal particles at fluid interfaces. *The European Physical Journal E*. **26**, 151–160 (2008).
16. Botto, L., Lewandowski, E. P., Cavallaro, M. & Stebe, K. J. Capillary interactions between anisotropic particles. *Soft Matter*. **8**, 9957–9971 (2012).
17. Lewandowski, E. P. et al. Orientation and self-assembly of cylindrical particles by anisotropic capillary interactions. *Langmuir*. **26**, 15142–15154 (2010).
18. Delens, M. & Vandewalle, N. Encoding quadrupolar capillary information into saddle-shaped objects for advanced self-assembly. *Soft Matter* (in review).
19. Reynolds, K., O'Riordan, A. & Redmond, G. Self-assembly of a functional electronic circuit directed by capillary interactions. *Applied Physics A*. **98**, 203–209 (2010).
20. Thomson, S. J., Barotta, J.-W. & Harris, D. M. Nonequilibrium capillary self-assembly (2023). arXiv: 2309.01668.
21. Grzybowski, B. A., Stone, H. A. & Whitesides, G. M. Dynamic self-assembly of magnetized, millimetre-sized objects rotating at a liquid-air interface. *Nature*. **405**, 1033–1036 (2000).
22. Vandewalle, N. et al. Symmetry breaking in a few-body system with magnetocapillary interactions. *Physical Review E*. **85**, 041402 (2012).
23. Hooshanginejad, A. et al. Interactions and pattern formation in a macroscopic magnetocapillary salr system of mermaid cereal. *Nature Communications*. **15**, 5466 (2024).
24. Davies, G. B. & Botto, L. Dipolar capillary interactions between tilted ellipsoidal particles adsorbed at fluid-fluid interfaces. *Soft Matter*. **11**, 7969–7976 (2015).
25. Kaneelil, P. R., de Souza, J. P., Turk, G., Pahlavan, A. A. & Stone, H. A. Electrically mediated self-assembly and manipulation of drops at an interface. *Soft Matter*. **20**, 5417–5424 (2024).
26. Grosjean, G. et al. Remote control of self-assembled microswimmers. *Scientific reports*. **5**, 1–8 (2015).
27. Collard, Y., Grosjean, G. & Vandewalle, N. Magnetically powered metachronal waves induce locomotion in self-assemblies. *Communications Physics*. **3**, 1–10 (2020).
28. Zeng, C. et al. 3d-printed machines that manipulate microscopic objects using capillary forces. *Nature*. **611**, 68–73 (2022).
29. Delens, M., Franckart, A. & Vandewalle, N. 3d-printed spines for programmable liquid topographies and micromanipulation. *Nature Communication*. **16**, 4348 (2025).
30. Jülicher, F., Ajdari, A. & Prost, J. Modeling molecular motors. *Reviews of Modern Physics*. **69**, 1269 (1997).
31. Poty, M., Lumay, G. & Vandewalle, N. Customizing mesoscale self-assembly with three-dimensional printing. *New Journal of Physics*. **16**, 023013 (2014).
32. Danov, K. D., Kralchevsky, P. A., Naydenov, B. N. & Brenn, G. Interactions between particles with an undulated contact line at a fluid interface: Capillary multipoles of arbitrary order. *Journal of colloid and interface science*. **287**, 121–134 (2005).
33. Domínguez Álvarez, Á., Oettel, M. & Dietrich, S. Force balance of particles trapped at fluid interfaces. *The Journal of Chemical Physics*. **128** (2008).
34. Kralchevsky, P. A. & Nagayama, K. Capillary forces between colloidal particles. *Langmuir*. **10**, 23–36 (1994).
35. Kralchevsky, P. A. & Nagayama, K. Capillary interactions between particles bound to interfaces, liquid films and biomembranes. *Advances in colloid and interface science*. **85**, 145–192 (2000).
36. Kralchevsky, P. A., Denkov, N. D. & Danov, K. D. Particles with an undulated contact line at a fluid interface: interaction between capillary quadrupoles and rheology of particulate monolayers. *Langmuir*. **17**, 7694–7705 (2001).
37. Brown, A., Smith, C. & Rennie, A. Fabricating colloidal particles with photolithography and their interactions at an air-water interface. *Physical Review E*. **62**, 951 (2000).
38. Stamou, D., Duschl, C. & Johannsmann, D. Long-range attraction between colloidal spheres at the air-water interface: The consequence of an irregular meniscus. *Physical Review E*. **62**, 5263 (2000).
39. Xie, Q., Davies, G. B., Günther, F. & Harting, J. Tunable dipolar capillary deformations for magnetic janus particles at fluid-fluid interfaces. *Soft Matter*. **11**, 3581–3588 (2015).
40. Xie, Q., Davies, G. B. & Harting, J. Controlled capillary assembly of magnetic janus particles at fluid-fluid interfaces. *Soft Matter*. **12**, 6566–6574 (2016).
41. Davies, G. B., Krüger, T., Coveney, P. V., Harting, J. & Bresme, F. Assembling ellipsoidal particles at fluid interfaces using switchable dipolar capillary interactions. arXiv preprint arXiv:1408.3140 (2014).
42. Davies, G. B., Krüger, T., Coveney, P. V., Harting, J. & Bresme, F. Interface deformations affect the orientation transition of magnetic ellipsoidal particles adsorbed at fluid-fluid interfaces. *Soft Matter*. **10**, 6742–6748 (2014).
43. Dörr, A. & Hardt, S. Driven particles at fluid interfaces acting as capillary dipoles. *Journal of Fluid Mechanics*. **770**, 5–26 (2015).
44. Wildeman, S. Real-time quantitative schlieren imaging by fast fourier demodulation of a checkered backdrop. *Experiments in Fluids*. **59**, 97 (2018).
45. Metzmacher, J., Lagubeau, G., Poty, M. & Vandewalle, N. Double pattern improves the schlieren methods for measuring liquid-air interface topography. *Experiments in Fluids*. **63**, 120 (2022).
46. Chan, D., Henry, J. Jr. & White, L. The interaction of colloidal particles collected at fluid interfaces. *J. Colloid Interface Sci.*. **79**, 410–418 (1981).

47. Allain, C. & Cloitre, M. Interaction between particles trapped at fluid interfaces: I. exact and asymptotic solutions for the force between two horizontal cylinders. *Journal of colloid and interface science*. **157**, 261–268 (1993).
48. Ravazzoli, P. D., Gonzalez, A. G., Diez, J. A. & Stone, H. A. Buoyancy and capillary effects on floating liquid lenses. *Phys. Rev. Fluids*. **5**, 073604 (2020).

Acknowledgements

This work is financially supported by the University of Liège through the CESAM Research Unit and by the FNRS CDR project number J.0186.23, entitled "Magnetocapillary Interactions for Locomotion at Liquid Interfaces" (MILLI).

Author contributions

J.M. conceived and conducted the experiments, J.M. analyzed the results, M.D. modeled the evolution of the capillary charge with the current, and J.M. simulated the interface. All authors wrote and reviewed the manuscript. N.V. supervised the project and secured funding.

Declarations

Competing interests

The authors declare no competing interests.

Additional information

Supplementary Information The online version contains supplementary material available at https://doi.org/10.1038/s41598-025-06413-y.

Correspondence and requests for materials should be addressed to N.V.